Transport dynamics of complex fluids

Sanggeun Song[a,b,c], Seong Jun Park[a,b,c], Minjung Kim[d], Jun Soo Kim[e], Bong June Sung[f], Sangyoub Lee[d], Ji-Hyun Kim[a,1], and Jaeyoung Sung[a,b,c,1]

[a]Creative Research Initiative Center for Chemical Dynamics in Living Cells, Chung-Ang University, 06974 Seoul, Republic of Korea; [b]Department of Chemistry, Chung-Ang University, 06974 Seoul, Republic of Korea; [c]National Institute of Innovative Functional Imaging, Chung-Ang University, 06974 Seoul, Republic of Korea; [d]Department of Chemistry, College of Natural Sciences, Seoul National University, 08826 Seoul, Republic of Korea; [e]Department of Chemistry and Nanoscience, Ewha Womans University, 03760 Seoul, Republic of Korea; and [f]Department of Chemistry, Sogang University, 04107 Seoul, Republic of Korea

Edited by Steve Granick, Institute for Basic Science Center for Soft and Living Matter, Ulju-gun, Ulsan, Republic of Korea, and approved May 9, 2019 (received for review January 7, 2019)

Thermal motion in complex fluids is a complicated stochastic process but ubiquitously exhibits initial ballistic, intermediate subdiffusive, and long-time diffusive motion, unless interrupted. Despite its relevance to numerous dynamical processes of interest in modern science, a unified, quantitative understanding of thermal motion in complex fluids remains a challenging problem. Here, we present a transport equation and its solutions, which yield a unified quantitative explanation of the mean-square displacement (MSD), the non-Gaussian parameter (NGP), and the displacement distribution of complex fluids. In our approach, the environment-coupled diffusion kernel and its time correlation function (TCF) are the essential quantities that determine transport dynamics and characterize mobility fluctuation of complex fluids; their time profiles are directly extractable from a model-free analysis of the MSD and NGP or, with greater computational expense, from the two-point and four-point velocity autocorrelation functions. We construct a general, explicit model of the diffusion kernel, comprising one unbound-mode and multiple bound-mode components, which provides an excellent approximate description of transport dynamics of various complex fluidic systems such as supercooled water, colloidal beads diffusing on lipid tubes, and dense hard disk fluid. We also introduce the concepts of intrinsic disorder and extrinsic disorder that have distinct effects on transport dynamics and different dependencies on temperature and density. This work presents an unexplored direction for quantitative understanding of transport and transport-coupled processes in complex disordered media.

complex fluids | thermal motion | diffusion kernel correlation | supercooled water | colloidal particles on lipid tube

Thermal motion in complex fluids is a complex stochastic process, which underlies a diverse range of dynamical processes of interest in modern science. Since Einstein's seminal work on Brownian motion (1), thermal motion in condensed media has been the subject of a great deal of research. However, it is still challenging to achieve a quantitative understanding of the transport dynamics of disordered fluidic systems, including cell nuclei and cytosols (2), membranes and biological tissue (3), polymeric fluid (4), supercooled water (5, 6), ionic liquids (7, 8), and dense hard-disk fluids (9). Interestingly, thermal motion of these complex fluids commonly exhibits a mean-square displacement (MSD) with initial ballistic, intermediate subdiffusive, and then terminal diffusive behavior (10–12); the associated displacement distribution is non-Gaussian except in the short- and long-time limits, and its deviation from Gaussian increases at short times but decreases at long times, as long as thermal motion is uninterrupted. These phenomena cannot be quantitatively explained by the original theory of Brownian motion (13).

To explain dynamics of anomalous thermal motion, the theory of Brownian motion has undergone a number of generalizations (14–27). Among these generalizations, Montroll and Weiss's (20) continuous-time random walk (CTRW) model enables quantitative description of anomalous transport caused by a tracer particle being trapped by other objects in disordered solid media (28); the CTRW with a power-law waiting-time distribution (WTD), $\psi(t) \propto t^{-(1+\alpha)}$ $(0 < \alpha < 1)$, successfully explains charge transport dynamics in amorphous semiconductors (29), which show a subdiffusive power-law MSD. These subdiffusive transport dynamics can be described by the fractional diffusion equation (30) or the fractional Fokker–Planck equation (31–33) in the continuum limit. Mandelbrot and Van Ness's (21) fractional Brownian motion (FBM) is another famous model of anomalous subdiffusive transport with a power-law MSD; however, FBM is a Gaussian subdiffusive process, while the CTRW with a power-law WTD is a non-Gaussian process. O'Shaughnessy and Procaccia (23) and Havlin and Ben-Avraham (24) investigate anomalous transport originating from self-similarity of transport media, considering random walks or diffusion in a fractal. Recently, Novikov et al. (34, 35) introduced a model of anomalous thermal motion dependent on mesoscopic structures of media and analyzed the long-time behavior of the diffusion coefficient by using a renormalization group solution.

While these models successfully describe subdiffusive transport occurring in disordered media, a number of disordered fluidic systems exhibit Fickian yet non-Gaussian diffusion (36–43); that is, the MSD is linearly proportional to time but the displacement distribution deviates from Gaussian. This issue was recently addressed by stochastic diffusivity (SD) models, in which the diffusion coefficient is treated as a stochastic variable (44–51). While SD models successfully demonstrate Fickian yet non-Gaussian diffusion, to the best of our knowledge, these models, too, are inconsistent with the transient subdiffusive MSD and the nonmonotonic time dependence of the non-Gaussian parameter (NGP), widely observed features of complex fluids.

Significance

Many disordered fluid systems exhibit anomalous transport dynamics, which do not obey Einstein's theory of Brownian motion or other currently available theories. Here, we present a new transport equation governing thermal motion of complex fluidic systems, which provides a unified, quantitative explanation of the mean-square displacement, the non-Gaussian parameter, and the displacement distribution of various complex fluids. The applicability of our theory is demonstrated for molecular dynamics simulation results of supercooled water and dense hard disc fluids and for experimental results of colloidal beads diffusing on lipid tubes. This work suggests previously unexplored directions for quantitative investigation into transport and transport-coupled processes in complex disordered media, including living cells.

Author contributions: J.S. designed research; S.S., S.J.P., J.S.K., B.J.S., S.L., J.-H.K., and J.S. performed research; S.S., S.J.P., M.K., and J.-H.K. analyzed data; and S.S., J.S.K., B.J.S., S.L., J.-H.K., and J.S. wrote the paper.

The authors declare no conflict of interest.

This article is a PNAS Direct Submission.

[1]To whom correspondence may be addressed. Email: jaeyoung@cau.ac.kr or jihyunkim@cau.ac.kr.

This article contains supporting information online at www.pnas.org/lookup/suppl/doi:10.1073/pnas.1900239116/-/DCSupplemental.

Published online June 7, 2019.

The NGP has a long history in transport theory. Rahman, Singwi, and Sjölander first noted that the NGP is an observable in neutron scattering experiments (52), and Rahman recognized it as the first-order coefficient in the Hermite-polynomial expansion of the displacement distribution around Gaussian (53). Nieuwenhuizen and Ernst (54) showed that the NGP, or the fourth cumulant of displacement, is related to the time-correlation function (TCF) of the diffusion coefficient fluctuation and the Burnett correlation function (BCF), a functional of velocity autocorrelation functions (VAFs), for a system of independent charged particles hopping on a one-dimensional lattice with static disorder. Later, the NGP and BCF were investigated for interacting gas and fluid systems (55, 56) and, more recently, also for glassy systems (57, 58) for which the authors suggested the NGP as a measure of the diffusion coefficient fluctuation and dynamic heterogeneity. However, for complex fluid systems commonly exhibiting initial ballistic and intermediate subdiffusive thermal motion before terminal diffusion, the TCF of the diffusion coefficient is neither well defined nor a good measure of mobility fluctuation before terminal diffusion emerges. For complex fluid systems exhibiting non-Fickian diffusion, there is no precise definition of mobility fluctuation or exact relationship of mobility fluctuation with the NGP and VAFs. Of course, it remains a challenge to achieve a unified, quantitative understanding of the anomalous MSD, nonmonotonic NGP, and non-Gaussian displacement distribution of various complex fluid systems.

Transport Equation of Complex Fluids

Here, to address these issues, we present a transport equation that provides a quantitative description of thermal motion for various complex fluids. This equation can be derived by considering the continuum limit of a random walk model with a general sojourn time distribution, $\psi_{\mathbf{\Gamma}}(t)$, coupled to arbitrary hidden environmental variables $\mathbf{\Gamma}$ (Fig. 1); $\mathbf{\Gamma}$ designates the entire set of dynamical variables that affect transport dynamics in disordered fluids. For this model, the joint probability, $p(m,\mathbf{\Gamma},t)$, that a random walker is located at the mth site and the environmental state is at $\mathbf{\Gamma}$ at time t can be written as (49, 59)

$$p(m,\mathbf{\Gamma},t)=\sum_{N=0}^{\infty}p(m|N)P_N(\mathbf{\Gamma},t). \qquad [1]$$

In Eq. **1**, $p(m|N)$ denotes the conditional probability that the random walker is located at the mth site, given that it has undergone N jumps, which is well known: $p(m|N)=(N!/m_+!m_-!)2^{-N}$ with $m_\pm=(N\pm m)/2$ $(N\geq|m|)$, and $p(m|N)=0$ $(N<|m|)$ (60). On the other hand, $P_N(\mathbf{\Gamma},t)$ denotes the joint probability that the total number of jumps made by the random walker is N and the environmental state is at $\mathbf{\Gamma}$ at time t. $P_N(\mathbf{\Gamma},t)$ is the crucial factor determining the time dependence of $p(m,\mathbf{\Gamma},t)$. Using a generalized version of Sung and Silbey's (61) master equation, which provides a formally exact description of the time evolution of $P_N(\mathbf{\Gamma},t)$, we derive the following transport equation from Eq. **1** in the continuum limit (*SI Appendix*, Text S1):

$$\hat{p}(\mathbf{r},\mathbf{\Gamma},s)=\hat{\mathcal{D}}_{\mathbf{\Gamma}}(s)\nabla^2\hat{p}(\mathbf{r},\mathbf{\Gamma},s)+L(\mathbf{\Gamma})\hat{p}(\mathbf{r},\mathbf{\Gamma},s). \qquad [2]$$

Here, $\hat{p}(\mathbf{r},\mathbf{\Gamma},s)$ and $\hat{p}(\mathbf{r},\mathbf{\Gamma},s)$ denote the Laplace transform of $\partial p(\mathbf{r},\mathbf{\Gamma},t)/\partial t$ and $p(\mathbf{r},\mathbf{\Gamma},t)$, respectively; $p(\mathbf{r},\mathbf{\Gamma},t)$ denotes the joint probability density that a particle is located at position $\mathbf{r}$ and the hidden environment is at state $\mathbf{\Gamma}$ at time t. This joint probability density satisfies the following normalization condition: $\int d\mathbf{r}\int d\mathbf{\Gamma}p(\mathbf{r},\mathbf{\Gamma},t)=1$. Throughout this work, $\hat{f}(s)$ denotes the Laplace transform of $f(t)$, i.e., $\int_0^\infty dte^{-st}f(t)$. In Eq. **2**, $\hat{\mathcal{D}}_{\mathbf{\Gamma}}(s)$ designates the diffusion kernel that is determined by the environmental state-dependent sojourn time distribution, $\psi_{\mathbf{\Gamma}}(t)$ of our random walk model; i.e., $\hat{\mathcal{D}}_{\mathbf{\Gamma}}(s)=\lim_{\varepsilon\to0}(\varepsilon^2/2d)s\hat{\psi}_{\mathbf{\Gamma}}(s)/[1-\hat{\psi}_{\mathbf{\Gamma}}(s)]=\lim_{\varepsilon\to0}\varepsilon^2\hat{\kappa}_{\mathbf{\Gamma}}(s)/2d$ with ε and d denoting the lattice constant and the spatial dimension, respectively. $\hat{\kappa}_{\mathbf{\Gamma}}(s)(\equiv s\hat{\psi}_{\mathbf{\Gamma}}(s)/[1-\hat{\psi}_{\mathbf{\Gamma}}(s)])$ denotes the jump rate kernel of the random walker, which is dependent on lattice constant ε; for the continuum limit description, we assume $\lim_{\varepsilon\to0}\varepsilon^2\hat{\kappa}_{\mathbf{\Gamma}}(s)$ exists. In Eq. **2**, $L(\mathbf{\Gamma})$ designates a mathematical operator describing the dynamics of the hidden environmental variables $\mathbf{\Gamma}$.

For the sake of generality, we do not assume a particular model of environmental state dynamics, nor do we assume a particular form of mathematical operator $L(\mathbf{\Gamma})$ at this point. A correct mathematical form of $L(\mathbf{\Gamma})$ is dependent on the environment surrounding the system in question; when environmental state dynamics are a non-Markov process, $L(\mathbf{\Gamma})$ may be dependent on Laplace variable s. As demonstrated in this work, quantitative information about transport dynamics coupled to hidden environmental variables can be extracted from simultaneous analysis of the MSD and NGP time profiles. This information can then be used to construct a more explicit model of transport dynamics of complex fluidic systems.

Eq. **2** encompasses the CTRW model and the diffusing diffusivity models (45–51) (see *Discussion* for more details). A further generalization of Eq. **2** for complex fluidic systems under a spatially heterogeneous external potential is presented in *SI Appendix*, Text S2.

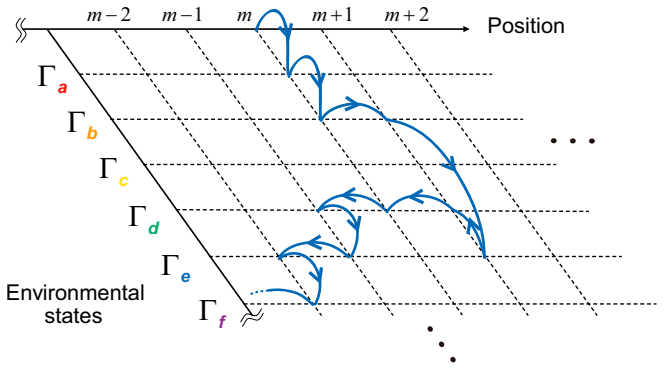

Fig. 1. Schematic representation of our random walk model with environmental state-dependent dynamics. In our model, the sojourn time distribution $\psi_{\mathbf{\Gamma}}(t)$ of a random walker is dependent on environmental state variables, $\mathbf{\Gamma}$. The probabilistic dynamics of this random walker model can be described by Eq. **2** in the continuum limit.

Analytic Expressions of the Moments

From Eq. **2**, we obtain the exact analytical expressions of the first two nonvanishing moments, $\langle|\mathbf{r}(t)-\mathbf{r}(0)|^2\rangle(\equiv\Delta_2(t))$ and $\langle|\mathbf{r}(t)-\mathbf{r}(0)|^4\rangle(\equiv\Delta_4(t))$, of the displacement distribution:

$$\hat{\Delta}_2(s)=\frac{2d}{s^2}\left\langle\hat{\mathcal{D}}_{\mathbf{\Gamma}}(s)\right\rangle, \qquad [3a]$$

$$\hat{\Delta}_4(s)=\left(1+\frac{2}{d}\right)2s\hat{\Delta}_2(s)^2\left[1+s\hat{C}_{\mathcal{D}}(s)\right]. \qquad [3b]$$

In obtaining Eqs. **3a** and **3b**, we assume that the hidden environment is initially in a stationary state, such as the equilibrium state or the nonequilibrium steady state (see *SI Appendix*, Text S3 for details). The bracket notation, $\langle\cdots\rangle$, designates the average over the stationary initial distribution of the environmental state. We can extend Eqs. **3a** and **3b** to the case where the initial state of the hidden environment is a nonstationary state, as is the case for glass, for which the analytic expressions of $\hat{\Delta}_2(s)$ and $\hat{\Delta}_4(s)$ are more complicated than Eqs. **3a** and **3b** (*SI Appendix*, Text S4). However, transport dynamics of various complex fluids can be quantitatively explained by Eqs. **3a** and **3b**, as demonstrated in this work. Hereafter, we focus on quantitative analysis of transport dynamics of complex fluidic systems with use of Eqs. **3a** and **3b**. We leave a quantitative explanation of transport dynamics in glass to future research.

The mean diffusion kernel, $\langle \mathcal{D}_\Gamma(t)\rangle$, in Eq. **3a** is nothing but the two-point VAF; i.e., $\langle \mathcal{D}_\Gamma(t)\rangle = \langle \mathbf{v}(t)\cdot\mathbf{v}(0)\rangle/d$ with $\mathbf{v}(t)$ being the velocity vector. This can be seen by comparing Eq. **3a** and the Laplace transform of the well-known relation, $\Delta_2(t) = 2\int_0^t d\tau_2 \int_0^{\tau_2} d\tau_1 \langle \mathbf{v}(\tau_2-\tau_1)\cdot\mathbf{v}(0)\rangle$ (62), exact as long as $\langle \mathbf{v}(\tau_2)\cdot\mathbf{v}(\tau_1)\rangle = \langle \mathbf{v}(\tau_2-\tau_1)\cdot\mathbf{v}(0)\rangle$. Knowing this and utilizing the Tauberian theorem, we obtain $\lim_{s\to\infty} s\langle \hat{\mathcal{D}}_\Gamma(s)\rangle = \lim_{t\to 0}\langle \mathbf{v}(t)\cdot\mathbf{v}(0)\rangle/d = \langle |\mathbf{v}|^2\rangle/d = k_BT/M$, with k_BT and M denoting thermal energy and the mass of our tracer particle, respectively. This means that $\langle \hat{\mathcal{D}}_\Gamma(s)\rangle$ is proportional to the mean-square velocity in the large-s limit; i.e., $\langle \hat{\mathcal{D}}_\Gamma(s)\rangle \cong s^{-1}\langle |\mathbf{v}|^2\rangle/d$ $(s\to\infty)$. On the other hand, in the small-s limit, the value of $\langle \hat{\mathcal{D}}_\Gamma(s)\rangle$ approaches $\int_0^\infty dt\langle \mathbf{v}(t)\cdot\mathbf{v}(0)\rangle/d$, which is simply the diffusion constant, $\bar{D}$, according to the Green–Kubo relation (63). Substituting the small (large)-s limit asymptotic behavior of $\langle \hat{\mathcal{D}}_\Gamma(s)\rangle$ into Eq. **3a**, we recover the well-known asymptotic behavior of the MSD: $d(k_BT/M)t^2$ at short times and $2d\bar{D}t$ at long times.

While the second moment, $\Delta_2(t)$, is dependent only on $\langle \mathcal{D}_\Gamma(t)\rangle$, the fourth moment, $\Delta_4(t)$, is dependent on the environment-coupled fluctuation of the diffusion kernel, $\mathcal{D}_\Gamma(t)$. In Eq. **3b**, $\hat{C}_\mathcal{D}(s)$ is the Laplace transform of the diffusion kernel correlation (DKC) or TCF of the diffusion kernel fluctuation (see *SI Appendix*, Eq. **S3-12** for the precise definition). At long times, where the MSD is linear in time, the diffusion kernel becomes the diffusion coefficient; i.e., $\hat{\mathcal{D}}_\Gamma(s)\cong\hat{\mathcal{D}}_\Gamma(0)(\equiv D_\Gamma)$ so that $C_\mathcal{D}(t)$ can be identified as the TCF of the diffusion coefficient fluctuation; i.e., $C_\mathcal{D}(t)\cong\langle \delta D(t)\delta D(0)\rangle/\langle D\rangle^2 = \eta_D^2\phi_D(t)$, where η_q^2 and $\phi_q(t)(q\in\{v^2, D\})$ designate the relative variance, $\langle \delta q^2\rangle/\langle q\rangle^2$, and the normalized TCF of q, $\langle \delta q(t)\delta q(0)\rangle/\langle \delta q^2\rangle$, respectively. At short times, on the other hand, $C_\mathcal{D}(t)$ can be identified as the TCF of squared speed $v^2(t)(\equiv|\mathbf{v}(t)|^2)$; i.e., $C_\mathcal{D}(t)\cong d\eta_{v^2}^2\phi_{v^2}(t)[=d\langle \delta v^2(t)\delta v^2(0)\rangle/\langle v^2\rangle^2]$ (*SI Appendix*, Text S5). Given that the initial speed distribution obeys the Maxwell–Boltzmann distribution, we obtain $\langle v^4\rangle = (1+2/d)\langle v^2\rangle^2$, and the initial value of $C_\mathcal{D}(t)$ can then only be given by $\lim_{t\to 0}C_\mathcal{D}(t) = d((\langle v^4\rangle - \langle v^2\rangle^2))/\langle v^2\rangle^2 = 2$. We find this is true for supercooled water and dense hard disk fluids (Fig. 2*D* and *SI Appendix*, Fig. S1*D*).

In our theory, $C_\mathcal{D}(t)$ is the essential dynamic quantity that characterizes environment-coupled mobility fluctuation. It serves as an ideal measure of mobility fluctuation for complex fluids exhibiting non-Fickian thermal motion, for which the TCF of the diffusion coefficient, the conventional measure of mobility fluctuation, is not well defined. As is shown below, there exists an exact relationship between $C_\mathcal{D}(t)$ and the four-point and two-point VAFs, valid at all times and at any spatial dimension.

Using Eqs. **3a** and **3b** and the definition of the NGP, $\alpha_2(t)[\equiv\Delta_4(t)/[(1+2/d)\Delta_2(t)^2]-1]$, we can quantitatively explain the MSD and NGP of various complex fluids. From the MSD and NGP data, we can extract the time profiles of $\langle \mathcal{D}_\Gamma(t)\rangle$ and $C_\mathcal{D}(t)$ either by assuming analytic functional forms for the MSD and NGP or without making any such assumption (*Methods*). In Fig. 2, we demonstrate our quantitative analysis of the molecular dynamics (MD) simulation results of the MSD and NGP for 4-point transferable intermolecular potential/2005 (TIP4P/2005) water (64), assuming specific analytic forms of the MSD and NGP but without assuming a particular model of the hidden environment or its influence on the diffusion kernel. As shown in this work, this information is useful in constructing an explicit model of transport dynamics of complex fluid systems; from this explicit model, we can predict or quantitatively understand the time dependence of the displacement distribution. Meanwhile, a model-free analysis of the MSD and NGP based on Eqs. **3a** and **3b** yields accurate and robust quantitative information about the time profiles of $\langle \mathcal{D}_\Gamma(t)\rangle$ and $C_\mathcal{D}(t)$, but, on its own, is not physically interpretable (Fig. 3).

Diffusion Kernel Correlation and Velocity Autocorrelation Functions

The diffusion kernel correlation, $C_\mathcal{D}(t)$, is closely related to the two- and four-point VAFs through the BCF. It is known that the NGP, $\alpha_2(t)$, or the fourth cumulant, $\mathrm{X}_4(t)[=(1+2/d)\Delta_2(t)^2\alpha_2(t) = \Delta_4(t) - (1+2/d)\Delta_2(t)^2]$, of displacement is related to the BCF, $\beta(t)$, by (54–56)

$$\mathrm{X}_4(t) = 4!d\int_0^t dt_1(t-t_1)\beta(t_1), \qquad [4]$$

where $\beta(t)$ is defined by

$$\beta(t_1) = \int_0^{t_1} dt_2 \int_0^{t_2} dt_3[\langle v_\alpha(0)v_\alpha(t_1)v_\alpha(t_2)v_\alpha(t_3)\rangle - \langle v_\alpha(0)v_\alpha(t_1)\rangle\langle v_\alpha(t_2)v_\alpha(t_3)\rangle - \langle v_\alpha(0)v_\alpha(t_2)\rangle\langle v_\alpha(t_1)v_\alpha(t_3)\rangle - \langle v_\alpha(0)v_\alpha(t_3)\rangle\langle v_\alpha(t_1)v_\alpha(t_2)\rangle]. \qquad [5]$$

In Eq. **5**, v_α indicates a Cartesian component of velocity vector, $\mathbf{v}$, and $\langle v_\alpha(0)v_\alpha(t_1)v_\alpha(t_2)v_\alpha(t_3)\rangle$ and $\langle v_\alpha(0)v_\alpha(t)\rangle[=(k_BT/M)\phi_{v_\alpha}(t)]$ denote the four- and two-point VAFs, respectively. According

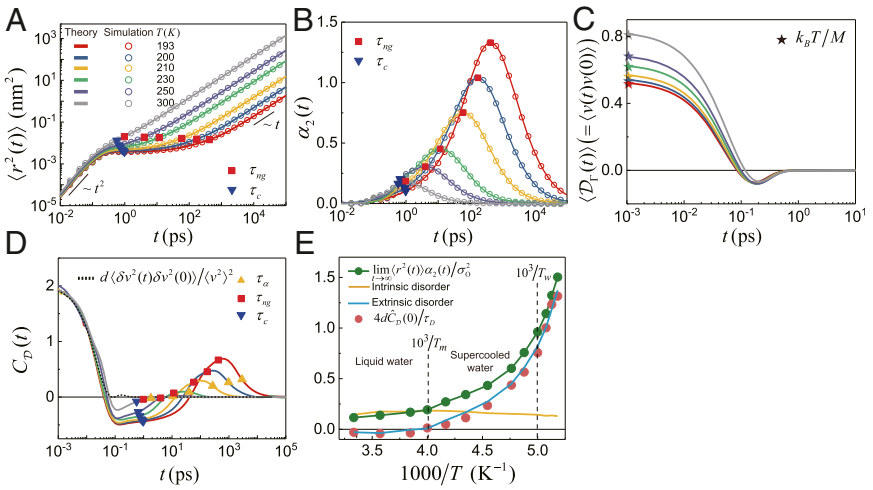

Fig. 2. Model-based quantitative analysis of the mean-square displacement (MSD) and non-Gaussian parameter (NGP) for the TIP4P/2005 water system. (*A* and *B*) Time profiles of the MSD and NGP at various temperatures. Open circles, simulation results; solid lines, the best fits of Eqs. **9** and **18** to the simulation results. (*C*) Mean diffusion kernel obtained from Eq. **10** with optimized parameter values. (*D*) Solid lines, diffusion kernel correlation, $C_\mathcal{D}(t)$, extracted from the MSD and NGP data (*Methods*); dotted line, the mean-scaled TCF of squared speed of supercooled water at 193 K (*SI Appendix*, Fig. S11). In *A*, *B*, and *D*, the navy-blue triangles and the red squares represent the caging times, τ_c, and the NGP peak times, τ_{ng}, respectively. In *D*, the yellow triangles represent the alpha relaxation times, τ_α (*SI Appendix*, Fig. S12). (*E*) Green circles, total disorder, $\lim_{t\to\infty}\langle r^2(t)\rangle\alpha_2(t)/\sigma_O^2$, with σ_O denoting an oxygen atom's Lennard-Jones diameter, 3.1589 Å; yellow and cyan lines, intrinsic and extrinsic disorder (see text below Eq. **8**); red circles, $4d\hat{C}_\mathcal{D}(0)/\tau_D$, where d, $\hat{C}_\mathcal{D}(0)$, and $\tau_D(=\sigma_O^2/\bar{D})$, respectively, denote the spatial dimension, the whole-time integration of $C_\mathcal{D}(t)$, and the diffusion timescale. T_m and T_W denote, respectively, the melting temperature (64) and the Widom line temperature (91, 92) (*SI Appendix*, Fig. S13).

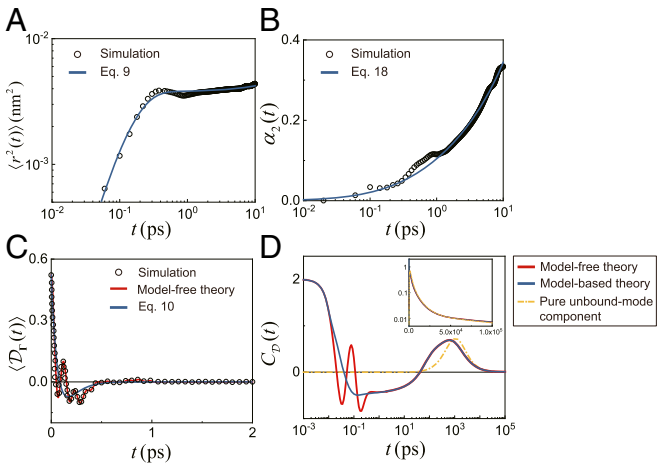

Fig. 3. Model-free quantitative analysis of the mean-square displacement (MSD) and non-Gaussian parameter (NGP) for the TIP4P/2005 water system at 193 K. (*A* and *B*) Time profiles of the MSD and NGP: circles, simulation results; blue lines, best fits of Eqs. **9** and **18**. (*C*) Mean diffusion kernel: circles, two-point VAF obtained from simulation; red line, second-order time derivative of MSD data; blue line, Eq. **10** with optimized parameters given in Table 1. (*D*) Time profile of diffusion kernel correlation extracted by analyzing the MSD and NGP data using (red line) model-free theory, (blue line) model-based theory, and (yellow dashed-dotted line) contribution of the unbound mode. (*D*, *Inset*) Time profile of $C_{\mathcal{D}}(t)$ in linear timescale. The difference between $C_{\mathcal{D}}(t)$ and the unbound-mode contribution results from the presence of the bound modes, accounted for by the second term on the R.H.S. of Eq. **12** (*SI Appendix*, Fig. S14).

to Wick's theorem, $\beta(t)$ vanishes when $v_\alpha(t)$ is a Gaussian process. Taking the Laplace transform of Eq. **4**, we obtain $\hat{X}_4(s) = \hat{\Delta}_4(s) - (1+2/d)\hat{\Delta}_2^2(s) = 4!d\,\hat{\beta}(s)/s^2$, where $\hat{\Delta}_2^2(s)$ denotes the Laplace transform of $\Delta_2(t)^2$. Substituting Eqs. **3a** and **3b** into the latter equation, we obtain an exact relation of the DKC to the BCF and the normalized VAF (see *SI Appendix*, Text S6 for the derivation):

$$\hat{C}_{\mathcal{D}}(s)\left\langle\hat{\mathcal{D}}_{\mathbf{\Gamma}}(s)\right\rangle^2 = \int_0^\infty dt e^{-st}\left[\frac{3}{2+d}\beta(t) + \left(\frac{k_BT}{M}\int_0^t dt'\phi_{v_\alpha}(t')\right)^2 + \frac{k_B^2T^2}{M^2}\int_0^t dt_1\int_0^{t_1} dt_2\left[\phi_{v_\alpha}(t) - \phi_{v_\alpha}(t-t_1)\right]\phi_{v_\alpha}(t_2)\right]. \quad [6]$$

Using Eq. **6** along with Eq. **5** and $\langle\hat{\mathcal{D}}_{\mathbf{\Gamma}}(s)\rangle = (k_BT/M)\hat{\phi}_{v_\alpha}(s)$, we can calculate the time profile of $C_{\mathcal{D}}(t)$ from the four- and two-point VAFs, as demonstrated in Fig. 4*B* for supercooled water at 193 K.

Ergodicity and Long-Time Limit of Diffusion Kernel Correlation and Non-Gaussian Parameter

For fluidic systems showing terminal Fickian diffusion, $C_{\mathcal{D}}(t)$ has the same long-time limit value as the NGP; i.e., $C_{\mathcal{D}}(\infty) = \alpha_2(\infty)$, which can be shown by using Eqs. **3a** and **3b** and the definition of the NGP (*SI Appendix*, Text S7). This result indicates that the long-time limit NGP value, $\alpha_2(\infty)$, vanishes for ergodic fluid systems for which the TCF, $C_{\mathcal{D}}(\infty)$, of the diffusion coefficient vanishes in the long-time limit. However, for nonergodic systems with finite $C_{\mathcal{D}}(\infty)$, $\alpha_2(\infty)$ may not vanish, either. Therefore, $\alpha_2(\infty)$ can serve as an ergodicity measure for fluidic systems exhibiting long-time Fickian diffusion (*SI Appendix*, Fig. S2), which was noted by Odagaki (65) for the glass formation process. There exist transport systems with anomalous diffusion, $\Delta_2(t) \propto t^\nu$, and weak-ergodicity breaking. For such systems, $\alpha_2(\infty)$ deviates from $C_{\mathcal{D}}(\infty)$; even if $C_{\mathcal{D}}(\infty) = 0$, $\alpha_2(\infty)$ is finite and given by $\alpha_2(\infty) = \nu\Gamma(\nu)^2/\Gamma(2\nu) - 1$ with $\Gamma(z)$ denoting the Gamma function defined by $\Gamma(z) = \int_0^\infty dt\, t^{z-1}e^{-t}$ (*SI Appendix*, Text S7). This result was previously reported by Odagaki and Hiwatari (66) on the basis of the so-called coherent-medium approximation, which corresponds to a vanishingly small DKC; i.e., $C_{\mathcal{D}}(t) = 0$. Finally, for nonergodic systems exhibiting anomalous diffusion, $\Delta_2(t) \propto t^\nu$, at long times, we find that the relationship between $C_{\mathcal{D}}(\infty)$ and $\alpha_2(\infty)$ deviates from the result for the weak-ergodicity breaking system; instead, $\alpha_2(\infty)$ is given by $\alpha_2(\infty) = \nu\Gamma(\nu)^2[1 + C_{\mathcal{D}}(\infty)]/\Gamma(2\nu) - 1$ (*SI Appendix*, Text S7). These results suggest that the finite value of $\alpha_2(\infty)$ can serve an alternative measure of nonergodicity, which is constant in time unlike the ergodicity-breaking (EB) parameter proposed by He, Burov, Metzler, and Barkai (67).

Intrinsic and Extrinsic Disorder

For ergodic fluid systems, the long-time limit value of the product between the MSD and NGP serves as a measure of disorder strength. This disorder strength measure is decomposable into intrinsic and extrinsic disorder. To show this, consider the long-time asymptotic behavior of the MSD and NGP:

$$\Delta_2(t) \cong 2d\bar{D}t + \Delta_c \quad (t \to \infty) \quad [7a]$$

$$\alpha_2(t) \cong \frac{2\hat{C}_{\mathcal{D}}(0) + \Delta_c/d\bar{D}}{t} \quad (t \to \infty). \quad [7b]$$

Eq. **7a** can be obtained by substituting the Maclaurin series of $\langle\hat{\mathcal{D}}_{\mathbf{\Gamma}}(s)\rangle$, $\langle\hat{\mathcal{D}}_{\mathbf{\Gamma}}(s)\rangle = (\varepsilon^2/2d)\langle\hat{\kappa}_{\mathbf{\Gamma}}(s)\rangle = (\varepsilon^2/2d) \times [\langle\hat{\kappa}_{\mathbf{\Gamma}}(s)\rangle + \langle\hat{\kappa}'_{\mathbf{\Gamma}}(s)\rangle s + \cdots]$, into Eq. **3a** and by taking the inverse Laplace transform of the resulting equation. We present the derivation of Eqs. **7a** and **7b** in *SI Appendix*, Text S7. In Eq. **7a**, Δ_c is given by $\Delta_c = 2\int_0^\infty dt\langle\mathcal{D}_{\mathbf{\Gamma}}(t)\rangle t = 2\int_0^\infty dt\langle\mathbf{v}(t)\cdot\mathbf{v}(0)\rangle t$ and vanishes only when the VAF decays infinitely fast or only when velocity is white noise. In our random walk model, Δ_c emerges whenever the waiting-time distribution is a nonexponential function (*SI Appendix*, Text S8). On the other hand, in Eq. **7b**, $\hat{C}_{\mathcal{D}}(0)[= \int_0^\infty dt C_{\mathcal{D}}(t)]$ emerges whenever the diffusion kernel or the waiting-time distribution is coupled to environmental variables.

From Eqs. **7a** and **7b**, we obtain the long-time limit value of the product of the MSD and NGP as

$$\lim_{t\to\infty}\langle r^2(t)\rangle\alpha_2(t) = 2\left[\Delta_c + 2d\bar{D}\hat{C}_{\mathcal{D}}(0)\right]. \quad [8]$$

We define the dimensionless disorder strength of complex fluids as $\lim_{t\to\infty}\langle r^2(t)\rangle\alpha_2(t)/\sigma^2$, with σ being the effective diameter of a tracer particle. Eq. **8** tells us that disorder strength has two different components, $2\Delta_c/\sigma^2$ and $4d\bar{D}\hat{C}_{\mathcal{D}}(0)/\sigma^2$, which originate from a finite relaxation time of the mean diffusion kernel and from environment-coupled fluctuation of the diffusion kernel, respectively. We designate the latter term extrinsic disorder, which is quite sensitive to temperature and density of the environment, as demonstrated in Fig. 2*E* and *SI Appendix*, Fig. S1*E*. On the other hand, we designate $2\Delta_c/\sigma^2$ intrinsic disorder, because this term persists even when environment-coupled fluctuation in transport dynamics is negligible.

Intrinsic disorder is far less sensitive to the temperature and density of media than extrinsic disorder and can be easily estimated from Eq. **7a**, the asymptotic long-time behavior of the MSD. Extrinsic disorder can be estimated by a direct numerical calculation of $4d\bar{D}\hat{C}_{\mathcal{D}}(0)/\sigma^2$ or, more simply, by subtracting intrinsic disorder from total disorder strength (Fig. 2*E*); i.e., $4d\bar{D}\hat{C}_{\mathcal{D}}(0)/\sigma^2 = [\lim_{t\to\infty}\langle r^2(t)\rangle\alpha_2(t) - 2\Delta_c]/\sigma^2$.

Disorder strength, defined in Eq. **8**, is directly related to the whole-time integration of the BCF; that is, $\lim_{t\to\infty}\langle r^2(t)\rangle\alpha_2(t)/2 = \Delta_c + 2d\bar{D}\hat{C}_{\mathcal{D}}(0) = \frac{6d}{2+d}\hat{\beta}(0)/\bar{D}$. This follows from the small-s limit

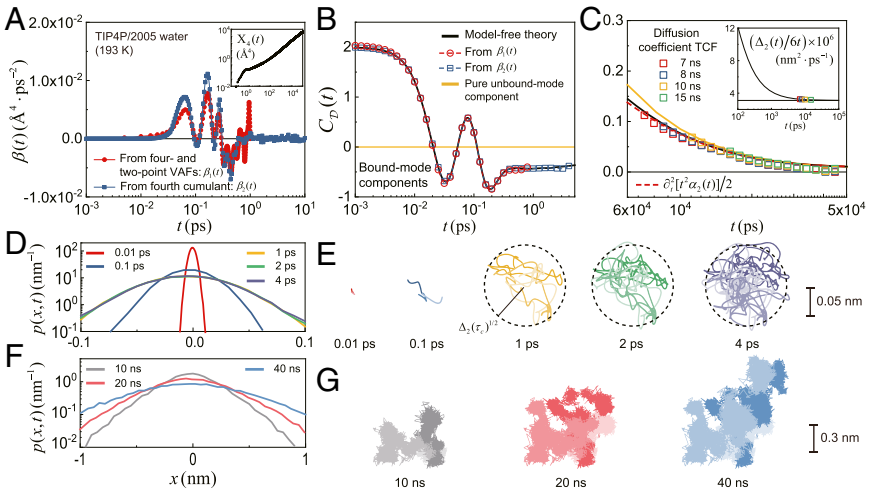

Fig. 4. Microscopic measurement of the bound- and unbound-mode components of diffusion kernel correlation for the TIP4P/2005 water system at 193 K. (*A*) Burnett correlation function (BCF): red circles, $\beta_1(t)$ obtained from Eq. **5** and the four- and two-point VAFs obtained from simulation; blue circles, $\beta_2(t)$ obtained from $\beta(t)=\partial_t^2 \mathrm{X}_4(t)/4!d$ and $\mathrm{X}_4(t)=(1+2/d)\Delta_2(t)^2\alpha_2(t)$. (*Inset*) The fourth cumulant, $\mathrm{X}_4(t)$, of displacement. (*B*) Short-time diffusion kernel correlation, $C_{\mathcal{D}}(t)$, obtained from (red circles) Eq. **6** and $\beta_1(t)$ and (blue circles) Eq. **6** and $\beta_2(t)$. (*C*) Long-time diffusion kernel correlation estimated by (squares) the mean-scaled TCF of diffusion coefficient fluctuation (*Methods*), (red dashed line) result of Eq. **14**, and (*Inset*) time dependence of MSD scaled by 6*t*. The simulation results of the diffusion coefficient fluctuation are calculated using various bin times, ranging from 7 ns to 15 ns. In *B* and *C*, the black and yellow lines represent, respectively, the result of model-free theory and the contribution of the unbound mode to $C_{\mathcal{D}}(t)$ shown in Fig. 3*D*. (*D*–*G*) Displacement distributions and representative time traces of three water molecules (*D* and *E*) at five different short times and (*F* and *G*) at three different long times. In *E* and *G*, the initial positions of all water molecules have been relocated to the center of the circle. In *E*, the dashed line represents a sphere centered at the initial position with radius $\Delta_2(\tau_c)^{1/2}$ (≈0.6 Å).

of $\hat{\mathrm{X}}_4(s)=\hat{\Delta}_4(s)-(1+2/d)\hat{\Delta}_2^2(s)=4!d\,\hat{\beta}(s)/s^2$, obtained from Eq. **4**, and from Eqs. **3a** and **3b** (*SI Appendix*, Text S6).

Model-Based Quantitative Analysis of the MSD and NGP

Intrinsic disorder causes the MSD to deviate from $2d\bar{D}t$, the prediction of the simple diffusion equation. We find that the following formula provides an excellent approximate description of the entire time range of the MSD for various disordered fluids (*SI Appendix*, Text S9):

$$\Delta_2(t)=2d\frac{k_BT}{M\gamma_0^2}c_0(\gamma_0 t-1+e^{-\gamma_0 t})+2d\frac{k_BT}{M}\sum_{i=1}^{n}\frac{c_i}{\omega_{0,i}^2}\left[1-e^{-\gamma_i t}\left(\cosh\omega_i t+\frac{\gamma_i}{\omega_i}\sinh\omega_i t\right)\right]. \quad [9]$$

This equation represents the MSD of a bead in a Gaussian polymer, but also quantitatively explains the MSD of liquid water and dense hard disk fluids (Fig. 2*A* and *SI Appendix*, Fig. S1*A*).

The applicability of Eq. **9** to various disordered fluid systems implies a universality in the MSD time profile of disordered fluids, which is decomposable into one unbound-mode dynamic and multiple bound-mode dynamics, comparable to viscoelastic motion of a bead in a polymer network. At short times, a tracer molecule is trapped by the surrounding molecules. This bound state consists of multiple bound modes, each with their own characteristic frequencies. Meanwhile, at long times, a tracer molecule escapes the cage of the surrounding molecules and moves around in the media, repeatedly being caged and escaping the cage. The first term on the right-hand side (R.H.S.) of Eq. **9** accounts for the unbound mode, and the second term accounts for the bound modes. In Eq. **9**, c_i and γ_i designate the weight coefficient and relaxation rate of the ith mode $(0\le i\le n)$. The weight coefficients are normalized by $\sum_{i=0}^{n}c_i=1$. $\omega_{0,i}$ is the natural frequency of the ith bound mode and is related to ω_i as $\omega_i=\sqrt{\gamma_i^2-\omega_{0,i}^2}$.

At all times, temperatures, and densities investigated, Eq. **9** with only two bound modes $(n=2)$ already provides a good quantitative explanation of the simulation results for the anomalous MSD of supercooled water and hard disk fluids (Fig. 2*A* and *SI Appendix*, Fig. S1*A*) and the experimental results for colloidal beads moving along lipid tubes (*SI Appendix*, Fig. S3) (36). According to Eq. **3a**, the analytic expression of the mean diffusion kernel yielding the MSD given in Eq. **9** can be obtained by

$$\left\langle\mathcal{D}_\Gamma(t)\right\rangle=\frac{k_BT}{M}c_0e^{-\gamma_0 t}+\frac{k_BT}{M}\sum_{i=1}^{n}c_ie^{-\gamma_i t}\left[\cosh(\omega_i t)-\frac{\gamma_i}{\omega_i}\sinh(\omega_i t)\right]. \quad [10]$$

Fig. 2*C* shows the mean diffusion kernel, or the VAF, calculated from Eq. **10** with parameter values optimized against MSD data from MD simulation shown in Fig. 2*A* for supercooled water.

The NGP is dependent not only on the mean transport dynamics, $\langle\hat{\mathcal{D}}_\Gamma(s)\rangle$, but also on fluctuation of transport dynamics, $C_{\mathcal{D}}(t)$. For simple diffusion, we have $\langle\hat{\mathcal{D}}_\Gamma(s)\rangle=\bar{D}$ and $C_{\mathcal{D}}(t)=0$, and Eqs. **3a** and **3b** yield $\Delta_2(t)=2d\bar{D}t$ and $\Delta_4(t)=(1+2/d)\Delta_2(t)^2$ so that the NGP vanishes. However, whenever $\langle\mathcal{D}_\Gamma(t)\rangle$ is not constant and/or $C_{\mathcal{D}}(t)\neq 0$, the NGP does not vanish. We find that, for disordered fluid systems investigated in this work, the time profiles of the NGP cannot be quantitatively understood when we neglect fluctuation in the diffusion kernel or when we assume $C_{\mathcal{D}}(t)=0$ (*SI Appendix*, Fig. S4).

The NGP of disordered fluids is a nonmonotonic function of time with a single peak. According to our model, the NGP quadratically increases with time, $\alpha_2(t)\propto t^2$ at short times (*SI Appendix*, Text S10 and Eq. **S10-9**), but decreases with time, $\alpha_2(t)\propto t^{-1}$, at long times following Eq. **7b**. As shown in Fig. 2*A*, it is only after the NGP peak time that Fickian diffusion emerges. These properties of the NGP are not specific to supercooled water but common across various disordered fluids (9, 12).

It was recently shown that diffusion coefficient fluctuation strongly correlates with string-like cooperative motion in dense fluids (57, 58), which is reportedly related to the NGP peak height (58). We find that the NGP peak height, $\alpha_2(\tau_{ng})$, serves as a measure of the relative variance of the diffusion coefficient for supercooled water. From the displacement distribution at the NGP peak time, we can extract the distribution of the diffusion coefficient using the method proposed in ref. 37. We find the relative variance, η_D^2, of the extracted diffusion coefficient distribution has the same value as the NGP peak height (*SI Appendix*, Fig. S5*D*). This is not a coincidence. We find the NGP peak height has the same value as the relative variance of the diffusion coefficient at the Fickian diffusion onset time or the NGP peak time, τ_{ng} (*SI Appendix*, Text S11). Both the NGP peak height and the NGP peak time increase with inverse temperature and density (Fig. 2*B* and *SI Appendix*, Fig. S1*B*).

Explicit Model for Diffusion Kernel

In the previous section, we demonstrated that the time profile of $C_{\mathcal{D}}(t)$ can be extracted from the MSD and the NGP based on Eqs. **3a** and **3b** using Eq. **9** for the MSD. To achieve a physical understanding of the time profile of $C_{\mathcal{D}}(t)$, we construct an explicit model of the environment-coupled diffusion kernel. Let us first consider the Laplace transform of Eq. **10**, $\langle \hat{\mathcal{D}}_{\mathbf{\Gamma}}(s)\rangle = c_0\hat{f}_0(s) + \sum_{i=1}^{n} c_i\hat{f}_i(s)$, where $\hat{f}_0(s)$ and $\hat{f}_i(s)$ denote the diffusion kernels associated with the unbound-mode dynamics and the ith bound-mode dynamics, given by $\hat{f}_0(s) = (k_BT/M)(s+\gamma_0)^{-1}$ and $\hat{f}_i(s) = (k_BT/M)s[(s+\gamma_i)^2 - \omega_i^2]^{-1}$, respectively. We can extend this equation by assuming the weight coefficients $\{c_0, c_1, \cdots, c_n\}$ are dependent on environmental state variables $\mathbf{\Gamma}$, obtaining the following model of the diffusion kernel:

$$\hat{\mathcal{D}}_{\mathbf{\Gamma}}(s) = c_0(\mathbf{\Gamma})\hat{f}_0(s) + \sum_{i=1}^{n} c_i(\mathbf{\Gamma})\hat{f}_i(s). \quad [11]$$

From this model, we obtain the analytic expression for $\hat{C}_{\mathcal{D}}(s)$ (*SI Appendix*, Text S12),

$$\hat{C}_{\mathcal{D}}(s) = \langle \hat{\mathcal{D}}_{\mathbf{\Gamma}}(s)\rangle^{-2}\left[\frac{\gamma_0^2\langle \delta D^2\rangle \hat{\phi}_D(s)}{(s+\gamma_0)^2} + \sum_{i=0}^{n}\sum_{j=0}^{n}{}'\hat{C}_{ij}(s)\hat{f}_i(s)\hat{f}_j(s)\right], \quad [12]$$

where the prime notation signifies that the sum excludes the term with $i=j=0$, and $C_{ij}(t)$ denotes the time correlation between weight coefficients; i.e., $C_{ij}(t) = \langle \delta c_i(t)\delta c_j(0)\rangle$. Noting that $\lim_{s\to 0}\hat{f}_0(s) = k_BT/M\gamma_0$ and $\lim_{s\to 0}\hat{f}_{i>0}(s) = 0$, we obtain $\hat{\mathcal{D}}_{\mathbf{\Gamma}}(s) \cong c_0(\mathbf{\Gamma})(k_BT/M\gamma_0)(\equiv D_{\Gamma})$ from Eq. **11** in the small-s regime, $s \ll \gamma_i$. Therefore, we can relate the weight coefficient TCF, $\langle \delta c_0(t)\delta c_0(0)\rangle$, of the unbound mode to the TCF of the diffusion coefficient fluctuation by $\langle \delta c_0(t)\delta c_0(0)\rangle = \langle \delta D(t)\delta D(0)\rangle (M\gamma_0/k_BT)^2$ at times longer than any element of $\{\gamma_i^{-1}\}$. We find that the largest element of $\{\gamma_i^{-1}\}$ is γ_0^{-1}, whose value has order of 1 ps for the unbound mode for supercooled water (Table 1). At times longer than the NGP peak time, τ_{ng}, which is greater than the largest velocity relaxation time, γ_0^{-1} (Fig. 2 *B* and *C*), the bound-mode terms are negligible compared with unbound-mode term, so that the first term on the R.H.S. of Eq. **12** contributes the most to the relaxation of diffusion kernel fluctuation, leaving us with $C_{\mathcal{D}}(t) \cong \phi_D(t)\eta_D^2$ $(t > \tau_{ng})$. This result indicates that the DKC becomes the TCF of the diffusion coefficient at long times. Using this result and recalling that $\eta_D^2 \cong \alpha_2(\tau_{ng})$ (*SI Appendix*, Fig. S5*D*), we can then extract $\phi_D(t)$ from the time profile of $C_{\mathcal{D}}(t)/\alpha_2(\tau_{ng})$ at times longer than the NGP peak time. The long-time tail of $C_{\mathcal{D}}(t)$ or $\phi_D(t)$ extracted from the MSD and NGP can be explained by an explicit model of the diffusion coefficient fluctuation described later in this work.

We note here that the whole-time integration of the diffusion kernel, $C_{\mathcal{D}}(t)$, the determining factor of extrinsic disorder, is mostly contributed from the unbound-mode component (*SI Appendix*, Fig. S6). The bound-mode contribution to $C_{\mathcal{D}}(t)$ has a comparable magnitude to the unbound-mode contribution, but has a negligibly smaller relaxation timescale than the unbound-mode contribution; consequently, the unbound-mode component makes the dominant contribution to $\hat{C}_{\mathcal{D}}(0) = \int_0^{\infty} dtC_{\mathcal{D}}(t)$. The major contributor to $C_{\mathcal{D}}(t)$ is the unbound mode at long times but the bound modes at short times. For example, for supercooled water at 193 K, the bound-mode components of $C_{\mathcal{D}}(t)$ are dominant at times shorter than 30 ps, and the unbound-mode component is dominant at times longer than 5 ns (Fig. 3*D*).

Table 1. Optimized values of adjustable parameters for supercooled water at 193 K

MSD (Eq. **9**)

$\{c_0, c_1\} = \{0.403, 6.28\} \times 10^{-4}$
$\{\gamma_0, \gamma_1, \gamma_2\} = \{1.16, 6.14, 11.9\}$ ps^{-1}
$\{\omega_{0,1}, \omega_{0,2}\} = \{0.35, 11.9\}$ ps^{-1}

$\phi_D(t)$ (*SI Appendix*, Eqs. **12** and **S13-3c**)

$\{\beta b_1, \beta b_2, \beta b_3\} = \{1.51, 21.2, 61.9\} \times 10^{-2}$
$\{\lambda_1, \lambda_2, \lambda_3\} = \{0.0761, 1.30, 5.84\} \times 10^{-1}$ ns^{-1}

The mean-square displacement (MSD) is analyzed by Eq. **9** with one unbound and two bound modes; that is, $n = 2$. c_i and γ_i designate the weight coefficient and relaxation rate of the ith mode. The zeroth mode is the unbound mode, while the first and second ones are bound modes. The second mode is dominant compared with the first one; i.e., $c_2 = 1 - c_0 - c_1 \cong 1.00$. The mean diffusion coefficient is given by $\langle D\rangle = c_0k_BT/M\gamma_0 \cong 3.1\text{nm}^2/\mu\text{s}$. $\omega_{0,i}$ denotes the natural frequency of the ith bound mode. At thermal equilibrium, the variance of a 3D harmonic oscillator's position is given by $3k_BT/M\omega^2$ with ω being the natural frequency of the oscillator. The SD of the tracer particle's position in the bound modes can be estimated as $(3\sum_{i=1,2}c_ik_BT/M\omega_{0,i}^2)^{1/2}$, whose value is 0.6 Å, close to the value of $\Delta_2(\tau_c)^{1/2}$ at caging time τ_c. The natural frequency, $\omega_{0,2}$, of the dominant bound mode is close to the peak frequency of intermolecular hydrogen bond bending motion (*SI Appendix*, Fig. S8). The long-time profile of the diffusion kernel correlation, $C_{\mathcal{D}}(t)$, is directly related to the TCF of the diffusion coefficient fluctuation, $C_{\mathcal{D}}(t) \cong \phi_D(t)\eta_D^2$. Here, $\phi_D(t)$ and η_D^2 are defined by $\phi_D(t) = \langle \delta D(t)\delta D(0)\rangle/\langle \delta D^2\rangle$ and $\eta_D^2 = \langle \delta D^2\rangle/\langle D\rangle^2$, respectively. For supercooled water, we model the activation energy, E, of the diffusion coefficient, $D = A\exp(-\beta E)$, as a random variable composed of three Ornstein–Uhlenbeck (OU) processes, $\{\Gamma_i\}$; that is, $\beta E = \beta\langle E\rangle + \sum_{i=1}^{3}\beta b_i\Gamma_i$ (*SI Appendix*, Eq. **S13-1**). λ_i designates the relaxation rate of the ith OU mode in the activation energy fluctuation, defined by $\langle \Gamma_i(t)\Gamma_j(0)\rangle = \delta_{ij}e^{-\lambda_j t}$ (*SI Appendix*, Eqs. **S13-1** and **S13-2**). The adjustable parameters are optimized by comparing η_D^2 and $\phi_D(t)$ with the NGP peak value, $\alpha_2(\tau_{ng})$, and the time profile of $C_{\mathcal{D}}(t)$ at long times (*SI Appendix*, Fig. S6 and Text S13). The relaxation time, $\int_0^{\infty} dt\phi_D(t)$, of the diffusion coefficient fluctuation is estimated to be 2.1 ns, comparable to the structural relaxation timescale, τ_α, 2.9 ns for supercooled water at 193 K.

Model-Free Quantitative Analysis of the MSD and NGP

By analyzing the numerical data of the time-dependent MSD and NGP using Eqs. **3a** and **3b**, we can extract the time profiles of the mean diffusion kernel and the DKC without assuming a physical model, such as Eq. **9**. In Fig. 3, we demonstrate this model-free analysis of the MSD and NGP data for supercooled water at 193 K (*Methods*).

According to our simulation, shown in Fig. 3*A*, the MSD of supercooled water exhibits oscillatory behavior with a slight bump and dip between 0.1 ps and 1 ps. This mysterious nonmonotonic oscillation in the MSD time profile of supercooled water was previously reported in the literature (5, 68, 69). We find the nonmonotonic MSD time dependence is unrelated to the finite-size effect and emerges not only under a constant temperature condition but also under the constant energy condition (*SI Appendix*, Fig. S7). The origin of the slight oscillation in the MSD time profile may be attributable to the intermolecular hydrogen-bond stretching vibration in supercooled water, which was previously identified in the quenched normal mode spectrum of the TIP4P/2005 water model at low temperatures (70) (*SI Appendix*, Fig. S8) and may also be the origin of the small oscillatory behavior in the NGP time profile between 0.1 ps and 1 ps (Fig. 3*B*). We find that these oscillations in the MSD and NGP time profiles are absent in liquid water above the melting temperature (Fig. 2*A*) and hard disk fluids (*SI Appendix*, Fig. S1*A*) at any density and cannot be accurately represented by Eqs. **9** and **18**, used for the model-based analysis of the MSD and NGP in the previous section.

The mean diffusion kernel and the diffusion kernel correlation extracted from the model-free analysis of the MSD and NGP transiently display oscillatory behaviors at times around 0.1 ps, which are more complicated than the behavior of their counterparts extracted using Eqs. **9** and **18** of the MSD and NGP (Fig. 3 *C* and *D*). However, at times shorter than 0.01 ps or longer than 0.4 ps, the model-free analysis yields essentially the same results as the model-based analysis. As shown in Fig. 3*D*, *Inset*,

both the model-free and model-based methods yield essentially the same result for the long-time DKC or the TCF of the diffusion coefficient fluctuation, quantitatively explainable by the unbound-mode component, or the first term on the R.H.S. of Eq. **12**, only. Consequently, both methods yield the same value for the whole-time integration of the DKC, or extrinsic disorder, $4d\bar{D}\tilde{C}_{\mathcal{D}}(0)/\sigma^2 (=[\lim_{t\to\infty}\langle r^2(t)\rangle\alpha_2(t) - 2\Delta_c]/\sigma^2)$, and hence for intrinsic disorder as well, because total disorder can only be the sum of intrinsic and extrinsic disorder.

Microscopic Measurement of the Bound- and Unbound-Mode Components of Diffusion Kernel Correlation

To test the correctness of our results in the previous sections, we perform an alternative, microscopic measurement of the mean diffusion kernel and DKC using MD simulation and compare the results with those obtained in the previous sections. We then show that the bound-mode and unbound-mode transport dynamics, separately embodied in our transport model, clearly manifest, respectively, on the short-time and long-time dependence of the displacement distribution and the spatial volume spanned by the MD simulation trajectories for supercooled water at 193 K.

The mean diffusion kernel and DKC calculated from the MD simulation results of the two- and four-point TCF are found to be in excellent agreement with those extracted from the MSD and NGP. This is demonstrated for an example of supercooled water at 193 K in Figs. 3 and 4.

The short-time DKC, dominantly contributed from the bound-mode component, can be directly calculated using Eq. **6** and the direct MD simulation results of the VAFs; the BCF appearing in Eq. **6** can be calculated from its definition, Eq. **5**. Note that the BCF can also be calculated from the MSD and NGP data, with use of the following relation: $\beta(t) = \partial_t^2 \mathrm{X}_4(t)/4!d$ and $\mathrm{X}_4(t) = (1+2/d)\ \Delta_2(t)^2\alpha_2(t)$. These two methods produce similar, noisy BCF time profiles as shown in Fig. 4*A* for supercooled water at 193 K. When substituted into Eq. **6**, these two BCF time profiles yield essentially the same results for the DKC, which is also in perfect agreement with the DKC extracted from our analysis of the MSD and NGP in the previous section (Fig. 4*D*).

We find that, at long times, the DKC is linearly proportional to the BCF (*SI Appendix*, Text S6):

$$C_{\mathcal{D}}(t) \cong \frac{3}{2+d}\,\beta(t)\Big/\bar{D}^2. \qquad [13]$$

Recalling that the DKC becomes the TCF of the diffusion coefficient fluctuation, $C_{\mathcal{D}}(t) \cong \phi_D(t)\eta_D^2 = \langle \delta D(t)\delta D(0)\rangle/\bar{D}^2$ at long times, we obtain the long-time approximation of Eq. **13** as $\langle \delta D(t)\delta D(0)\rangle \cong 3\beta(t)/(d+2)$. This result tells us that, for a one-dimensional system, the BCF is the same as the diffusion coefficient fluctuation, which was previously recognized by Nieuwenhuizen and Ernst (54) and others (71, 72) for a one-dimensional system of independent charged particles hopping on a lattice with static disorder. Our result here indicates that the long-time BCF has the same time profile as the long-time DKC multiplied by $(d+2)/3$, which is shown in Fig. 3*D*, *Inset*. It is not easy to calculate the long-time profile of the BCF directly from its definition, Eq. **5**, because of the large computational expense involved in accurately estimating the multipoint VAFs from MD simulation and the 2D integral appearing in Eq. **5**.

An independent estimation of the long-time DKC can be made by using MD simulations to measure the diffusion coefficient fluctuation along each time trace and calculating the TCF of the diffusion coefficient (*Methods*). This is because the DKC becomes the diffusion coefficient at long times, as mentioned earlier. In Fig. 4*C*, for supercooled water at 193 K, we show that $\eta_D^2\phi_D(t)$ calculated from direct MD simulation is actually in good agreement with the long-time profile of $C_{\mathcal{D}}(t)$ extracted from the MSD and NGP data. The long-time DKC is dominantly contributed from the unbound-mode component, or the first term on the R.H.S. of Eq. **12**, as shown in Fig. 4*C*.

An alternative estimation of the long-time DKC can be made from the time profile of the NGP. The long-time DKC is directly related to the NGP and its time derivatives as follows:

$$C_{\mathcal{D}}(t) \cong \frac{1}{2}\frac{\partial^2}{\partial t^2}\left[t^2\alpha_2(t)\right] = \alpha_2(t) + 2t\dot{\alpha}_2(t) + 2^{-1}t^2\ddot{\alpha}(t). \qquad [14]$$

This equation can be obtained by substituting the long-time expression of the fourth cumulant, $\mathrm{X}_4(t) \cong (1+2/d)(2d\bar{D}t)^2\alpha_2(t)$, into the well-known equation, $\beta(t) = \partial_t^2\mathrm{X}_4(t)/4!d$, and then substituting the result into Eq. **13**. Eq. **14** tells us that the NGP carries the complete information about the long-time relaxation of mobility fluctuation of complex fluids. As shown in Fig. 4*C* for supercooled water at 193 K, the long-time DKC estimated by Eq. **14** quantitatively agrees with the long-time DKC obtained from three other methods, namely, extraction from the MSD and NGP data, using Eq. **6** and MD simulation results of the VAF, and MD simulation of the diffusion coefficient fluctuation and calculation of its TCF.

Bound-mode (unbound-mode) transport dynamics are reflected on the time dependence of the displacement distribution at short (long) times. For supercooled water at 193 K, the displacement distribution broadens rapidly before 1 ps but after this does not greatly change for several picoseconds (Fig. 4*D*). This bound-mode feature of transport dynamics also manifests itself on the time-dependent volume spanned by the MD simulation trajectories of a water molecule. As shown in Fig. 4*E*, the spatial volume spanned by the simulation trajectories rapidly increases with time before 1 ps, but afterward, this trajectory volume tends to saturate to a certain critical value over several picoseconds while the trajectory length continues increasing with time. In contrast, at long-time scales, the displacement distribution and the trajectory volume exhibit unbound-mode dynamics, as demonstrated in Fig. 4 *F* and *G*.

Quantitative Explanation of Fickian Yet Non-Gaussian Displacement Distribution

Disordered fluids exhibit non-Gaussian diffusion; that is, the displacement distribution is non-Gaussian even at long times where the MSD linearly increases with time (9, 12, 36–38). The displacement distribution of disordered fluids starts as Gaussian with variance given by $\mathbf{r}(\Delta t) - \mathbf{r}(0) \cong \mathbf{v}(0)\Delta t$ at short times but deviates at any finite time. At the NGP peak time, where the deviation from Gaussian is greatest, the displacement distribution often appears similar to a Laplace distribution with an exponential tail (50). It is at this time that the non-Gaussian displacement distribution begins its relaxation to Gaussian and the MSD becomes linear in time. This phenomenon is widely observed across various disordered fluid systems (7, 9, 12), but has yet to be quantitatively explained.

To understand the time-dependent relaxation of the non-Gaussian displacement distribution in the Fickian diffusion regime, we need an explicit model of the diffusion coefficient fluctuation for the fluid system in question. In the literature, the diffusion coefficient is often modeled as $D = A\exp(-\beta E)$, where A, β, and E are the entropic factor, inverse thermal energy, and activation energy, respectively (73). This model can be generalized by assuming that the entropic factor and activation energy are stochastic variables dependent on hidden environmental variables. In this work, we make this generalization and consider two exactly solvable models.

The first model assumes that the diffusion coefficient is given by $D_{\mathbf{\Gamma}} = A_{\mathbf{\Gamma}}\exp(-\beta E_{\mathbf{\Gamma}})$, where the fluctuation of $E_{\mathbf{\Gamma}}$ around its mean value, $\langle E_{\mathbf{\Gamma}}\rangle$, is given by $E_{\mathbf{\Gamma}}(t) - \langle E\rangle = \sum_k b_k\Gamma_k(t)$, where $\{b_k\}$ and $A_{\mathbf{\Gamma}}$ are constants and $\{\Gamma_k\}$ are stationary Gaussian Markov processes, also known as Ornstein–Uhlenbeck (OU) processes, satisfying $\langle \Gamma_k(t)\Gamma_l(0)\rangle = \delta_{kl}\exp(-\lambda_k t)$ (*SI Appendix*, Text S13) (74). For this model, exact analytic expressions of $\langle D\rangle$, η_D^2, and $\phi_D(t)\eta_D^2$ can be obtained (Table 1 legend and *SI Appendix*, Eq. **S13-3**), where the adjustable parameters are optimized against the diffusion coefficient

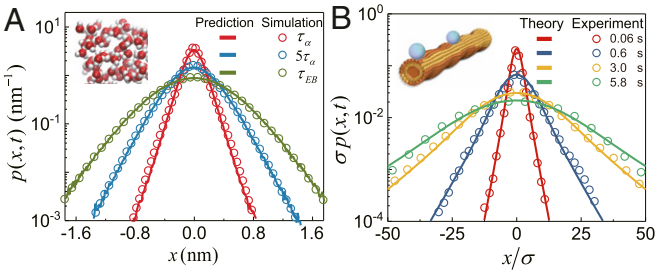

Fig. 5. Quantitative explanation of displacement distributions for supercooled water and colloidal beads on lipid tubes. (*A*) Displacement distributions of a water molecule along a Cartesian coordinate at three different times, τ_α(≅2.9ns), $5\tau_\alpha$(≅14.4ns), and τ_{EB}(≅36.4ns). Circles, simulation results for TIP4P/2005 water at 193 K; lines, theoretical predictions of our first model. (*B*) Scaled displacement distribution of colloidal beads with diameter σ along a lipid tube at various times. Circles, experimental results reported in ref. 36; lines, theoretical results of our second model (*SI Appendix*, Texts S12 and S14).

value, the NGP peak value, and the long-time DKC data (*SI Appendix*, Text S13). The optimized parameter values are presented in Table 1. Using the first model with optimized parameter values, we can now predict the time-dependent relaxation of the non-Gaussian displacement distribution in the Fickian diffusion regime (*SI Appendix*, Text S13). The prediction of this model is in excellent agreement with the MD simulation results for the displacement distribution of supercooled water, as shown in Fig. 5*A*.

In the second model, we model the diffusion coefficient as $D_{\mathbf{\Gamma}}(t) = A_{\mathbf{\Gamma}}(t)\exp(-\beta E_{\mathbf{\Gamma}}(t)) \cong \langle D\rangle \sum_k a_k \Gamma_k^2(t)$, where $\{a_k\}$ and $\{\Gamma_k(t)\}$ are constants and OU processes, respectively. This is a generalization of the model in ref. 47 and yields an analytic expression of the displacement distribution (Table 2 legend and *SI Appendix*, Eq. **S14-3**). We find this expression provides an excellent quantitative explanation of the experimentally measured displacement distribution of colloidal beads diffusing on lipid tubes reported in ref. 36 (Fig. 5*B*). The optimized parameters of the second model are presented in Table 2. Eq. **12** with optimized parameter values allows us to calculate the time profiles of the DKC for the colloidal bead system (Table 2 legend and *SI Appendix*, Fig. S3).

The displacement distribution approaches a Gaussian distribution only after individual displacement trajectories become statistically equivalent. If individual displacement trajectories are statistically equivalent, the EB parameter proposed by He, Burov, Metzler, and Barkai (67) is linear in $t/t_{\max}$, where t and $t_{\max}$ denote the time lag, or the interval over which the time-averaged MSD is calculated, and the maximum trajectory length, respectively (75). Otherwise, the EB parameter deviates from its linear dependence on $t/t_{\max}$. At temperatures lower than 230 K, the EB parameter of supercooled water shows an anomalous power-law dependence on $t/t_{\max}$ at short times but resumes normal linear dependence on $t/t_{\max}$ at times longer than the characteristic time τ_{EB} (*SI Appendix*, Fig. S9). Deviation of the displacement distribution from Gaussian becomes negligible only at times much longer than τ_{EB}, as demonstrated in *SI Appendix*, Fig. S9*B* for supercooled water. On the other hand, $C_{\mathcal{D}}(t)$ is negligibly small at the characteristic time τ_{EB} (*SI Appendix*, Fig. S9*B*). This is due to the fact that the long-time relaxation of the NGP is contributed not only from extrinsic disorder leading to the trajectory-to-trajectory variation in the transport dynamics, but also from intrinsic disorder, whose effects persist even for homogeneous systems with statistically equivalent displacement trajectories (Eq. **7b**). This analysis shows that the long-time tail of $C_{\mathcal{D}}(t)$ better characterizes the relaxation of diffusivity fluctuation than the NGP (76).

Discussion

Main Findings. We derived a transport equation, Eq. **2**, describing stochastic thermal motion of various complex fluids, which yields exact analytic results, Eqs. **3a** and **3b**, that enable a unified, quantitative explanation of not only the MSD but also the NGP time profiles of various complex fluids (Fig. 2 and *SI Appendix*, Fig. S1). The central dynamic quantity governing transport dynamics of complex fluids is the environment-dependent diffusion kernel. The mean diffusion kernel (MDK) and DKC can be unambiguously extracted from the MSD and NGP time profiles (Fig. 3 and *SI Appendix*, Fig. S1). We also established an exact relationship of the MDK and DKC with the two-point and four-point VAFs (Eqs. **4**–**6**), allowing for alternative, microscopic measurements of the MDK and DKC using MD simulation (Fig. 4 *A*–*C*). DKC is an ideal measure of mobility fluctuation of complex fluids exhibiting non-Fickian diffusion and is simply related to the NGP by Eq. **14**, at long times (Fig. 4*C*).

We constructed a physical model of the environment-coupled diffusion kernel (Eqs. **10**–**12**), composed of one unbound mode and multiple bound modes. This model provides a quantitative explanation of the MSD, NGP, and displacement distribution for various complex fluidic systems (Figs. 2 and 5 and *SI Appendix*, Fig. S1). Our model-based analysis of the frequency spectrum of the VAF suggests that the slight oscillation in supercooled water's MSD originates from intramolecular hydrogen bond stretching motion. We introduced the notion of intrinsic disorder and extrinsic disorder for complex fluid systems in Eq. **8**, which originate from a finite relaxation time of the mean diffusion kernel and the environment-coupled fluctuation of the diffusion kernel, respectively. We demonstrated a separate estimation of intrinsic and extrinsic disorder for supercooled water (Fig. 2*E*) and dense hard disk fluids (*SI Appendix*, Fig. S1*E*). Extrinsic disorder is more sensitive to temperature and density of complex fluids than intrinsic disorder; extrinsic disorder increases with inverse temperature and density, unless the complex fluids enter a solid-like phase.

Table 2. Optimized values of adjustable parameters for colloidal bead diffusion on lipid tubes

Colloidal beads on lipid tubes	Value
Displacement distribution (*SI Appendix*, Eq. **S14-3**)	
a_1, a_2	4.02×10^{-1}, $1 - a_1$
λ_1, λ_2 (Hz)	3.43, 1.04×10^{-2}

The experimental data are reported in ref. 36. We analyzed the displacement distribution data using our second model, $D_{\mathbf{\Gamma}}(t) \cong \langle D\rangle \sum_k a_k \Gamma_k^2(t)$ with $\langle \Gamma_k(t)\Gamma_j(0)\rangle = \delta_{jk}\exp(-\lambda_k t)$ (*SI Appendix*, Eq. **S14-1**), for which the displacement distribution in the Fourier domain is obtained as $\bar{p}(k,t) (\equiv \int_{-\infty}^{\infty} dx e^{ikx} p(x,t)) = \prod_{j=1}^{2} [4q_j e^{-(q_j-1)\lambda_j t} / \{(q_j+1)^2 - (q_j-1)^2 e^{-2q_j\lambda_j t}\}]^{1/2}$ with $q_j = (1 + 4a_j k^2 \langle D\rangle \lambda_j^{-1})^{1/2}$, where a_i is a parameter characterizing the relative contribution of Γ_k to diffusion coefficient fluctuation (*SI Appendix*, Eqs. **S14-2a**, **S14-2b**, and **S14-3**). The displacement distribution quantitatively explains the experimental data (Fig. 4*B*). This system exhibits Fickian diffusion in the experimental timescale. The diffusion constant is estimated to be $\langle D\rangle/\sigma^2 \cong 41.5$Hz with σ being the diameter of a colloidal bead. Using the optimized parameter values, we can calculate the NGP and the TCF of diffusion coefficient fluctuation, $\phi_D(t)$ using Eqs. **12** and *SI Appendix*, Eq. **S14-2b** (*SI Appendix*, Fig. S3). The relaxation time, $\int_0^\infty dt \phi_D(t) [= \sum_{i=1,2} a_i^2 \lambda_i^{-1} / 2(a_1^2 + a_2^2)]$, of the diffusion coefficient fluctuation is estimated to be 33.2 s. This value is comparable to the relaxation time, 3.48 ~ 34.8 s, of the lipid-tube membrane fluctuation under the zero shear stress condition (93); i.e., $\omega^{-1}(q) = [\langle z\rangle^3 q^2 (\kappa q^4 + \mu q^2)/3\eta]^{-1}$, at the smallest wavenumber, $q = 3 \times 10^5$ m^{-1} (36), where the values of the average tube diameter, $\langle z\rangle$, the bending stiffness, κ, and the surface tension, μ, are reported as 100 nm, 10^{-19} J, and $10^{-4} \sim 10^{-5}$ J·m^{-2}, respectively. η denotes the viscosity of the bulk water, whose value is given by 0.94 cP at 22 ~ 23 °C. This agreement between the values of $\int_0^\infty dt \phi_D(t)$ and $\omega^{-1}(q)$ implies that non-Gaussian diffusion results from the diffusion coefficient fluctuation caused by thermal fluctuation of the lipid tube into which colloidal beads are embedded, as discussed in ref. 36.

Comparison with Previous Models. Our model-based analysis of DKC is reminiscent of the memory kernel analyses by Berne, Boon, and Rice (77) and Douglas and Hubbard (78). Our random walk model is a generalization of the CTRW model, to account for environment-coupled fluctuation of transport dynamics. We refer to Shlesinger's review (79) on the origins and applications of the CTRW model. Our model reduces to the CTRW when $C_{\mathcal{D}}(t)=0$; both models yield the same MSD but different NGPs (*SI Appendix*, Figs. S2*E* and S4). For the CTRW model, the NGP is given by $\alpha_2(t)\cong -2/3 \ (t\to 0)$ (*SI Appendix*, Eq. **S10-4**); $(\Delta_c/d\bar{D})t^{-1}$ $(t\to\infty)$. The MSD of a random walker is dependent on the initial condition; non-Fickian diffusion of complex fluids cannot be modeled by a random walker model with a stationary initial condition (*SI Appendix*, Fig. S10 and Text S15).

Our transport equation, Eq. **2**, encompasses the SD model, which accounts for extrinsic disorder but neglects intrinsic disorder. Eq. **2** reduces to the transport equation of the SD model when the diffusion kernel is replaced by the diffusion coefficient. The MSD and NGP of the SD model are given by $\Delta_2(t)=2d\bar{D}t$ and $\alpha_2(t)\cong\eta_D^2 \ (t\to 0)$; $2\eta_D^2\hat{\phi}_D(0)t^{-1} \ (t\to\infty)$ (*SI Appendix*, Text S11), which cannot describe complex fluids with a non-Fickian MSD and initially vanishing NGP.

Potential Applications and Limitation. Our transport equation can be extended for complex fluids under an external potential field or for nonergodic fluids such as glass (*SI Appendix*, Texts S2 and S4). It can be further generalized for dynamics of transport-coupled reactions in complex fluids (80–82), which we leave for future research. Our MSD model in Eq. **9** is only approximate in the sense that it cannot capture weak oscillation in the MSD of supercooled water and the asymptotic long-time power-law relaxation of the two-point VAF of dense fluids (83–86). Improving our model to capture these phenomena is another future research topic.

In our transport equation, the diffusion kernel is independent of the absolute position of the tracer particle. However, by applying the projection operator technique (19, 87) to the Liouville equation, one can obtain a similar transport equation (*SI Appendix*, Text S16) but with the diffusion kernel dependent on the absolute position of the tracer particle, potentially important for a system with position-dependent transport dynamics. In most fluid systems, however, thermal motion is independent of the absolute position of the tracer particle.

For a more extensive discussion, see *SI Appendix*, Text S17, which we present at the request of an anonymous reviewer.

Outlook

The essential feature of our approach to transport dynamics of complex fluids is hidden environmental variables that represent the entire set of dynamic variables affecting transport dynamics of our tracer particles. By accounting for their effects without using an a priori explicit model, this approach enables the extraction of robust, quantitative information about the transport dynamics of complex fluid systems. This information can then be used to construct a more explicit model of the environment-coupled diffusion kernel, $\hat{\mathcal{D}}_{\mathbf{\Gamma}}(s)$, which has proved to be useful in quantitative interpretation and prediction of the MSD, NGP, and displacement distribution of various complex fluid systems. In achieving quantitative understanding of complex systems, this type of approach is advantageous over the conventional approach that relies on fully explicit models of the system, the environment, and their interactions. This is because, for a system interacting with a complex environment, it is difficult to construct a model that is both accurate and explicit from the outset, due to lack of information. Our approach is applicable and extendable to quantitative investigation of various other complex systems in natural science (88, 89).

Methods

Extraction of Diffusion Kernel Correlation from MSD and NGP. Here, we present the procedure for extracting the DKC, $C_{\mathcal{D}}(t)$, from the MSD and NGP obtained by computer simulation, where $C_{\mathcal{D}}(t)$ is defined by *SI Appendix*, Eq. **S3-12** in the Laplace domain. From *SI Appendix*, Eq. **S3-12**, we can represent $\hat{C}_{\mathcal{D}}(s)$ in terms of the first two nonvanishing moments as follows:

$$\hat{C}_{\mathcal{D}}(s)=\frac{\hat{\Delta}_4(s)}{\left(1+\frac{2}{d}\right)2s^2\hat{\Delta}_2(s)^2}-\frac{1}{s}. \qquad [15]$$

On the other hand, the NGP, $\alpha_2(t)$, is defined by

$$\alpha_2(t)=\frac{\Delta_4(t)}{\left(1+\frac{2}{d}\right)\Delta_2(t)^2}-1, \qquad [16]$$

which can be rearranged with respect to the fourth moment, $\Delta_4(t)$, as

$$\Delta_4(t)=\left(1+\frac{2}{d}\right)\Delta_2(t)^2[1+\alpha_2(t)]. \qquad [17]$$

The simulation results for the MSD and NGP are well represented by Eq. **9** with two bound modes ($n=2$) and a linear combination of three or four Gaussian-shaped functions given by

$$\alpha_2(t)\cong\sum_{i=1}^{3\text{ or }4}a_i\exp\left[-(\log_{10}t-b_i)^2\Big/c_i\right], \qquad [18]$$

respectively. We perform the best fits of Eqs. **9** and **18** to the simulation results for the MSD and NGP. By substituting the optimized results into Eq. **17**, we obtain the analytic expression of $\Delta_4(t)$ as a function of time. Taking the Laplace transforms of the best fitted $\Delta_2(t)$ and $\Delta_4(t)$, and substituting the results into Eq. **15**, we obtain the Laplace transform of $C_{\mathcal{D}}(t)$ for a given set of MSD and NGP data. Here, we can directly use the model-free results for the MSD and NGP obtained from the simulation, instead of using the model-based fits. To obtain the value of $C_{\mathcal{D}}(t)$ at a given time, t, we perform the numerical Laplace inversion of Eq. **15** using the Stehfest algorithm (90).

Generation of Time Traces of Fluctuating Diffusion Coefficient. Along the ith particle trajectory, $N+1$ displacements, $\mathbf{r}_i(t_e+t_j)-\mathbf{r}_i(t_j)$, with the same elapsed time, t_e, but different starting times, $\{t_j|k\le j\le N+k\}$, are selected. Here, $\{t_j\}$ are successive time sequences with a constant spacing, 2 ps. The elapsed time, t_e, must be long enough to capture Fickian diffusion. As shown in Fig. 4*C*, *Inset*, the MSD of a TIP4P/2005 water molecule at 193 K becomes fully linear in time beyond roughly 10 ns. From the selected displacements, the time-local MSD, $\Delta_2^{(i)}(t_e;t_k)=N^{-1}\sum_{j=k}^{N+k}[\mathbf{r}_i(t_j+t_e)-\mathbf{r}_i(t_j)]^2$, conditioned on time t_k for the ith particle trajectory is calculated. $\Delta_2^{(i)}(t_e;t_k)/6t_e$ is then assigned as a diffusion coefficient, $D^{(i)}(t_k)$, at time t_k (54, 71, 72). The resulting mean-scaled TCF, $\langle\delta D(t)\delta D(0)\rangle/\langle D\rangle^2$, obtained with $N=20$ and several elapsed times around 10 ns are well superimposed on each other (Fig. 4*C*). Here, the elapsed time, t_e, must be smaller than t as noted in ref. 71. It is also verified that the mean-scaled TCF obtained with $N=10$ or 30 is essentially the same as the result with $N=20$. When $t_e=10$ ns, the values of mean, $\langle D\rangle$, and relative variance, η_D^2, for the diffusion coefficient are estimated to be 3.2×10^{-6} m^2·s^{-1} and 1.2, respectively, consistent with $\bar{D}=\lim_{t\to\infty}\Delta_2(t)/6t=3.1\times10^{-6}$ m^2·s^{-1} and $\alpha_2(\tau_{ng})=1.3$.

ACKNOWLEDGMENTS. We gratefully acknowledge Professors Mike Shlesinger, Eli Barkai, Ralf Metzler, YounJoon Jung, and Jae-Hyung Jeon for their helpful comments and Mr. Luke Bates for his careful reading of our manuscript. This work was supported by the Creative Research Initiative Project program (2015R1A3A2066497) and the National Research Foundation of Korea Grant (2015R1A2A1A15055664) funded by the Korean government. S.S. also acknowledges the Chung-Ang University Graduate Research Scholarship in 2016.

1. A. Einstein, On the motion of small particles suspended in liquids at rest required by the molecular-kinetic theory of heat. *Ann. Phys. (Leipzig)* **17**, 549–560 (1905).
2. C. Di Rienzo, V. Piazza, E. Gratton, F. Beltram, F. Cardarelli, Probing short-range protein Brownian motion in the cytoplasm of living cells. *Nat. Commun.* **5**, 5891 (2014).
3. Y. Golan, E. Sherman, Resolving mixed mechanisms of protein subdiffusion at the T cell plasma membrane. *Nat. Commun.* **8**, 15851 (2017).
4. M. Doi, S. Edwards, Dynamics of concentrated polymer systems. Part 1.—Brownian motion in the equilibrium state. *J. Chem. Soc. Faraday Trans.* **74**, 1789–1801 (1978).
5. F. Sciortino, P. Gallo, P. Tartaglia, S. Chen, Supercooled water and the kinetic glass transition. *Phys. Rev. E Stat. Phys. Plasmas Fluids Relat. Interdiscip. Topics* **54**, 6331–6343 (1996).
6. S. D. Overduin, G. N. Patey, An analysis of fluctuations in supercooled TIP4P/2005 water. *J. Chem. Phys.* **138**, 184502 (2013).

7. M. G. Del Pópolo, G. A. Voth, On the structure and dynamics of ionic liquids. *J. Phys. Chem. B* **108**, 1744–1752 (2004).
8. Z. Hu, C. J. Margulis, Heterogeneity in a room-temperature ionic liquid: Persistent local environments and the red-edge effect. *Proc. Natl. Acad. Sci. U.S.A.* **103**, 831–836 (2006).
9. J. Kim, C. Kim, B. J. Sung, Simulation study of seemingly Fickian but heterogeneous dynamics of two dimensional colloids. *Phys. Rev. Lett.* **110**, 047801 (2013).
10. L. Larini, A. Ottochian, C. De Michele, D. Leporini, Universal scaling between structural relaxation and vibrational dynamics in glass-forming liquids and polymers. *Nat. Phys.* **4**, 42 (2008).
11. P. Charbonneau, Y. Jin, G. Parisi, F. Zamponi, Hopping and the Stokes-Einstein relation breakdown in simple glass formers. *Proc. Natl. Acad. Sci. U.S.A.* **111**, 15025–15030 (2014).
12. B. van der Meer, W. Qi, J. Sprakel, L. Filion, M. Dijkstra, Dynamical heterogeneities and defects in two-dimensional soft colloidal crystals. *Soft Matter* **11**, 9385–9392 (2015).
13. N. Wax, *Selected Papers on Noise and Stochastic Processes* (Courier Dover Publications, 1954).
14. Mv. Smoluchowski, Versuch einer mathematischen theorie der koagulationskinetik kolloider lösungen. *Z. Phys. Chem.* **92**, 129–168 (1918).
15. L. Onsager, Initial recombination of ions. *Phys. Rev.* **54**, 554 (1938).
16. P. Debye, Reaction rates in ionic solutions. *Trans. Electrochem. Soc.* **82**, 265–272 (1942).
17. P. E. Rouse, Jr, A theory of the linear viscoelastic properties of dilute solutions of coiling polymers. *J. Chem. Phys.* **21**, 1272–1280 (1953).
18. B. H. Zimm, Dynamics of polymer molecules in dilute solution: Viscoelasticity, flow birefringence and dielectric loss. *J. Chem. Phys.* **24**, 269–278 (1956).
19. H. Mori, Transport, collective motion, and Brownian motion. *Prog. Theor. Phys.* **33**, 423–455 (1965).
20. E. W. Montroll, G. H. Weiss, Random walks on lattices. II. *J. Math. Phys.* **6**, 167–181 (1965).
21. B. B. Mandelbrot, J. W. Van Ness, Fractional Brownian motions, fractional noises and applications. *SIAM Rev.* **10**, 422–437 (1968).
22. K. Kawasaki, Kinetic equations and time correlation functions of critical fluctuations. *Ann. Phys.* **61**, 1–56 (1970).
23. B. O'Shaughnessy, I. Procaccia, Analytical solutions for diffusion on fractal objects. *Phys. Rev. Lett.* **54**, 455–458 (1985).
24. S. Havlin, D. Ben-Avraham, Diffusion in disordered media. *Adv. Phys.* **36**, 695–798 (1987).
25. J. Klafter, A. Blumen, M. F. Shlesinger, Stochastic pathway to anomalous diffusion. *Phys. Rev. A Gen. Phys.* **35**, 3081–3085 (1987).
26. M. F. Shlesinger, G. M. Zaslavsky, J. Klafter, Strange kinetics. *Nature* **363**, 31–37 (1993).
27. B. Berkowitz, H. Scher, Theory of anomalous chemical transport in random fracture networks. *Phys. Rev. E Stat. Phys. Plasmas Fluids Relat. Interdiscip. Topics* **57**, 5858 (1998).
28. J. Klafter, R. Silbey, Derivation of the continuous-time random-walk equation. *Phys. Rev. Lett.* **44**, 55 (1980).
29. H. Scher, E. W. Montroll, Anomalous transit-time dispersion in amorphous solids. *Phys. Rev. B* **12**, 2455 (1975).
30. W. Wyss, The fractional diffusion equation. *J. Math. Phys.* **27**, 2782–2785 (1986).
31. R. Metzler, E. Barkai, J. Klafter, Anomalous diffusion and relaxation close to thermal equilibrium: A fractional Fokker-Planck equation approach. *Phys. Rev. Lett.* **82**, 3563 (1999).
32. E. Barkai, R. Metzler, J. Klafter, From continuous time random walks to the fractional Fokker-Planck equation. *Phys. Rev. E Stat. Phys. Plasmas Fluids Relat. Interdiscip. Topics* **61**, 132–138 (2000).
33. E. Barkai, CTRW pathways to the fractional diffusion equation. *Chem. Phys.* **284**, 13–27 (2002).
34. D. S. Novikov, E. Fieremans, J. H. Jensen, J. A. Helpern, Random walk with barriers. *Nat. Phys.* **7**, 508–514 (2011).
35. D. S. Novikov, J. H. Jensen, J. A. Helpern, E. Fieremans, Revealing mesoscopic structural universality with diffusion. *Proc. Natl. Acad. Sci. U.S.A.* **111**, 5088–5093 (2014).
36. B. Wang, S. M. Anthony, S. C. Bae, S. Granick, Anomalous yet Brownian. *Proc. Natl. Acad. Sci. U.S.A.* **106**, 15160–15164 (2009).
37. B. Wang, J. Kuo, S. C. Bae, S. Granick, When Brownian diffusion is not Gaussian. *Nat. Mater.* **11**, 481–485 (2012).
38. J. Guan, B. Wang, S. Granick, Even hard-sphere colloidal suspensions display Fickian yet non-Gaussian diffusion. *ACS Nano* **8**, 3331–3336 (2014).
39. S.-W. Park, S. Kim, Y. Jung, Time scale of dynamic heterogeneity in model ionic liquids and its relation to static length scale and charge distribution. *Phys. Chem. Chem. Phys.* **17**, 29281–29292 (2015).
40. J.-H. Jeon, M. Javanainen, H. Martinez-Seara, R. Metzler, I. Vattulainen, Protein crowding in lipid bilayers gives rise to non-Gaussian anomalous lateral diffusion of phospholipids and proteins. *Phys. Rev. X* **6**, 021006 (2016).
41. S. Kim, S.-W. Park, Y. Jung, Heterogeneous dynamics and its length scale in simple ionic liquid models: A computational study. *Phys. Chem. Chem. Phys.* **18**, 6486–6497 (2016).
42. N. Tyagi, B. J. Cherayil, Non-Gaussian Brownian diffusion in dynamically disordered thermal environments. *J. Phys. Chem. B* **121**, 7204–7209 (2017).
43. S. Acharya, U. K. Nandi, S. Maitra Bhattacharyya, Fickian yet non-Gaussian behaviour: A dominant role of the intermittent dynamics. *J. Chem. Phys.* **146**, 134504 (2017).
44. C. Beck, E. G. Cohen, Superstatistics. *Physica A* **322**, 267–275 (2003).
45. S. Hapca, J. W. Crawford, I. M. Young, Anomalous diffusion of heterogeneous populations characterized by normal diffusion at the individual level. *J. R. Soc. Interface* **6**, 111–122 (2009).
46. M. V. Chubynsky, G. W. Slater, Diffusing diffusivity: A model for anomalous, yet Brownian, diffusion. *Phys. Rev. Lett.* **113**, 098302 (2014).
47. R. Jain, K. L. Sebastian, Diffusion in a crowded, rearranging environment. *J. Phys. Chem. B* **120**, 3988–3992 (2016).
48. T. J. Lampo, S. Stylianidou, M. P. Backlund, P. A. Wiggins, A. J. Spakowitz, Cytoplasmic RNA-protein particles exhibit non-Gaussian subdiffusive behavior. *Biophys. J.* **112**, 532–542 (2017).
49. A. V. Chechkin, F. Seno, R. Metzler, I. M. Sokolov, Brownian yet non-Gaussian diffusion: From superstatistics to subordination of diffusing diffusivities. *Phys. Rev. X* **7**, 021002 (2017).
50. V. Sposini, A. V. Chechkin, F. Seno, G. Pagnini, R. Metzler, Random diffusivity from stochastic equations: Comparison of two models for Brownian yet non-Gaussian diffusion. *New J. Phys.* **20**, 043044 (2018).
51. J. Ślęzak, R. Metzler, M. Magdziarz, Superstatistical generalised Langevin equation: Non-Gaussian viscoelastic anomalous diffusion. *New J. Phys.* **20**, 023026 (2018).
52. A. Rahman, K. Singwi, A. Sjölander, Theory of slow neutron scattering by liquids. *I. Phys. Rev.* **126**, 986 (1962).
53. A. Rahman, Correlations in the motion of atoms in liquid argon. *Phys. Rev.* **136**, A405 (1964).
54. T. M. Nieuwenhuizen, M. Ernst, Excess noise in a hopping model for a resistor with quenched disorder. *J. Stat. Phys.* **41**, 773–801 (1985).
55. J. McLennan, Burnett coefficients and correlation functions. *Phys. Rev. A* **8**, 1479 (1973).
56. I. De Schepper, H. Van Beyeren, M. Ernst, The nonexistence of the linear diffusion equation beyond Fick's law. *Physica* **75**, 1–36 (1974).
57. H. Zhang, J. F. Douglas, Glassy interfacial dynamics of Ni nanoparticles: Part I Colored noise, dynamic heterogeneity and collective atomic motion. *Soft Matter* **9**, 1254–1265 (2013).
58. W.-S. Xu, J. F. Douglas, K. F. Freed, Influence of cohesive energy on relaxation in a model glass-forming polymer melt. *Macromolecules* **49**, 8355–8370 (2016).
59. I. M. Sokolov, J. Klafter, From diffusion to anomalous diffusion: A century after Einstein's Brownian motion. *Chaos* **15**, 26103 (2005).
60. S. Chandrasekhar, Stochastic problems in physics and astronomy. *Rev. Mod. Phys.* **15**, 1–89 (1943).
61. J. Sung, R. J. Silbey, Counting statistics of single molecule reaction events and reaction dynamics of a single molecule. *Chem. Phys. Lett.* **415**, 10–14 (2005).
62. H. Risken, *The Fokker-Planck Equation* (Springer, 1996), pp. 63–95.
63. R. Kubo, The fluctuation-dissipation theorem. *Rep. Prog. Phys.* **29**, 255–284 (1966).
64. J. L. Abascal, C. Vega, A general purpose model for the condensed phases of water: TIP4P/2005. *J. Chem. Phys.* **123**, 234505 (2005).
65. T. Odagaki, Non-ergodicity and non-Gaussianity in vitrification process. *Prog. Theor. Phys. Suppl.* **126**, 9–12 (1997).
66. T. Odagaki, Y. Hiwatari, Stochastic model for the glass transition of simple classical liquids. *Phys. Rev. A* **41**, 929–937 (1990).
67. Y. He, S. Burov, R. Metzler, E. Barkai, Random time-scale invariant diffusion and transport coefficients. *Phys. Rev. Lett.* **101**, 058101 (2008).
68. P. Gallo, M. Rovere, Mode coupling and fragile to strong transition in supercooled TIP4P water. *J. Chem. Phys.* **137**, 164503 (2012).
69. T. Kawasaki, K. Kim, Identifying time scales for violation/preservation of Stokes-Einstein relation in supercooled water. *Sci. Adv.* **3**, e1700399 (2017).
70. S. Saito, B. Bagchi, Thermodynamic picture of vitrification of water through complex specific heat and entropy: A journey through "no man's land". *J. Chem. Phys.* **150**, 054502 (2019).
71. C. Stanton, M. Nelkin, Random-walk model for equilibrium resistance fluctuations. *J. Stat. Phys.* **37**, 1–16 (1984).
72. A. Y. Smirnov, A. A. Dubkov, Anomalous non-Gaussian diffusion in small disordered rings. *Physica A* **232**, 145–161 (1996).
73. K. Krynicki, C. D. Green, D. W. Sawyer, Pressure and temperature dependence of self-diffusion in water. *Faraday Discuss. Chem. Soc.* **66**, 199–208 (1978).
74. G. E. Uhlenbeck, L. S. Ornstein, On the theory of the Brownian motion. *Phys. Rev.* **36**, 823–841 (1930).
75. W. Deng, E. Barkai, Ergodic properties of fractional Brownian-Langevin motion. *Phys. Rev. E Stat. Nonlin. Soft Matter Phys.* **79**, 011112 (2009).
76. T. Uneyama, T. Miyaguchi, T. Akimoto, Fluctuation analysis of time-averaged mean-square displacement for the Langevin equation with time-dependent and fluctuating diffusivity. *Phys. Rev. E Stat. Nonlin. Soft Matter Phys.* **92**, 032140 (2015).
77. B. J. Berne, J. P. Boon, S. A. Rice, On the calculation of autocorrelation functions of dynamical variables. *J. Chem. Phys.* **45**, 1086–1096 (1966).
78. J. F. Douglas, J. B. Hubbard, Semiempirical theory of relaxation: Concentrated polymer solution dynamics. *Macromolecules* **24**, 3163–3177 (1991).
79. M. F. Shlesinger, Origins and applications of the Montroll-Weiss continuous time random walk. *Eur. Phys. J. B* **90**, 93 (2017).
80. J. Sung, E. Barkai, R. J. Silbey, S. Lee, Fractional dynamics approach to diffusion-assisted reactions in disordered media. *J. Chem. Phys.* **116**, 2338–2341 (2002).
81. J. Sung, R. J. Silbey, Exact dynamics of a continuous time random walker in the presence of a boundary: Beyond the intuitive boundary condition approach. *Phys. Rev. Lett.* **91**, 160601 (2003).
82. K. Seki, M. Wojcik, M. Tachiya, Fractional reaction-diffusion equation. *J. Chem. Phys.* **119**, 2165–2170 (2003).
83. B. Alder, T. Wainwright, Decay of the velocity autocorrelation function. *Phys. Rev. A* **1**, 18 (1970).
84. M. Ernst, E. Hauge, J. Van Leeuwen, Asymptotic time behavior of correlation functions. *Phys. Rev. Lett.* **25**, 1254 (1970).
85. J. Dorfman, E. Cohen, Velocity correlation functions in two and three dimensions. *Phys. Rev. Lett.* **25**, 1257 (1970).
86. B. Choi *et al.*, Nature of self-diffusion in two-dimensional fluids. *New J. Phys.* **19**, 123038 (2017).
87. R. Zwanzig, Memory effects in irreversible thermodynamics. *Phys. Rev.* **124**, 983–992 (1961).
88. Y. R. Lim *et al.*, Quantitative understanding of probabilistic behavior of living cells operated by vibrant intracellular networks. *Phys. Rev. X* **5**, 031014 (2015).
89. S. J. Park *et al.*, The Chemical Fluctuation Theorem governing gene expression. *Nat. Commun.* **9**, 297 (2018).
90. H. Stehfest, Algorithm 368: Numerical inversion of Laplace transforms [D5]. *Commun. ACM* **13**, 47–49 (1970).
91. J. L. Abascal, C. Vega, Widom line and the liquid-liquid critical point for the TIP4P/2005 water model. *J. Chem. Phys.* **133**, 234502 (2010).
92. R. S. Singh, J. W. Biddle, P. G. Debenedetti, M. A. Anisimov, Two-state thermodynamics and the possibility of a liquid-liquid phase transition in supercooled TIP4P/2005 water. *J. Chem. Phys.* **144**, 144504 (2016).
93. N. Gov, A. G. Zilman, S. Safran, Hydrodynamics of confined membranes. *Phys. Rev. E Stat. Nonlin. Soft Matter Phys.* **70**, 011104 (2004).